Fluctuations in populations of subsurface methane oxidizers in coordination with changes in electron acceptor availability

C. Magnabosco[1*], P.H.A. Timmers[2], M.C.Y. Lau[3], G. Borgonie[4], B. Linage-Alvarez[5], O. Kuloyo[5,6], R. Alleva[7], T.L. Kieft[8], G.F. Slater[9], E. van Heerden[5,10], B. Sherwood Lollar[11], T.C. Onstott[3]

[1]Flatiron Institute Center for Computational Biology, Simons Foundation, New York USA
[2]Department of Microbial Physiology, Laboratory of Microbiology, Wageningen University, Wageningen Netherlands
[3]Department of Geosciences, Princeton University, Princeton USA
[4]Extreme Life Isyensya, Gentbrugge Belgium
[5] Department of Microbial, Biochemical and Food Biotechnology, University of the Free State Bloemfontein, South Africa
[6]Department of Geoscience, University of Calgary, Calgary Canada
[7]Department of Ecology and Evolutionary Biology, Princeton University, Princeton USA
[8]Department of Biology, New Mexico Institute of Mining and Technology, Socorro USA
[9]School of Geography and Earth Sciences, McMaster University, Hamilton Canada
[10]Biosaense Solutions, Bloemfontein, South Africa
[11]Department of Earth Sciences, University of Toronto, Toronto Canada
*To whom correspondence should be addressed: Cara Magnabosco; 162 Fifth Ave, New York, NY 10012
cmagnabosco@flatironinstitute.org; +1 646-603-3683

Running Title: Subsurface ANME in South Africa

Abstract:

The concentrations of electron donors and acceptors in the terrestrial subsurface biosphere fluctuate due to migration and mixing of subsurface fluids, but the mechanisms and rates at which microbial communities respond to these changes are largely unknown. Subsurface microbial communities exhibit long cellular turnover times and are often considered relatively static—generating just enough ATP for cellular maintenance. Here, we investigated how subsurface populations of CH_4 oxidizers respond to changes in electron acceptor availability by monitoring the biological and geochemical composition in a 1,339 meters-below-land-surface (mbls) fluid-filled fracture over the course of both longer (2.5 year) and shorter (2-week) time scales. Using a combination of metagenomic, metatranscriptomic, and metaproteomic analyses, we observe that the CH_4 oxidizers within the subsurface microbial community change in coordination with electron acceptor availability over time. We then validate these findings through a series of ^{13}C-CH_4 laboratory incubation experiments, highlighting a connection between composition of subsurface CH_4 oxidizing communities and electron acceptor availability.

Introduction:

The terrestrial subsurface is an energy-limited environment that is subject to changes in fluid chemistry over time (Onstott *et al.* 2006). Laboratory experiments have shown that when native fluids are supplemented with electron acceptors such as SO_4^{2-}, the activity of subsurface communities can be enhanced (Rajala *et al.* 2015). Large disturbances such as CO_2 (Morozova *et al.* 2010, 2011) and H_2 injection (Bagnoud *et al.* 2016), hydraulic fracking (Daly *et al.* 2016), and drilling (Purkamo *et al.* 2013) have also

49 been reported to alter natural subsurface communities. The response of microbial
50 communities to natural fluctuations in their environment, however, is less understood.
51   In the South African subsurface, increases in the availability of electron acceptors
52 such as NO_3^- (>10-fold higher) and SO_4^{2-} (>5-fold higher) over a 1.5 year period did not
53 correspond to changes in the bacterial community (Magnabosco *et al.* 2014; Simkus *et al.*
54 2015). However, 16S SSU rRNA gene amplicon surveys of the archaeal communities
55 from the same site and sampling points of the aforementioned studies showed a diverse
56 collection of anaerobic methane oxidizing archaea (ANME) (Young *et al.* 2017) and
57 methane oxidizing bacteria (Simkus *et al.* 2015).
58   ANME-1 and "*Candidatus* Methanoperedens nitroreducens", a member of
59 ANME-2d, are among the best described ANME and couple the oxidation of CH_4 with
60 SO_4^{2-} and NO_3^- reduction, respectively (Haroon *et al.* 2013; Wegener *et al.* 2015). Other
61 ANME-2d have also been reported to couple CH_4 oxidation to the reduction of Mn^{4+}
62 and/or Fe^{3+} (Ettwig *et al.* 2016). With the exception of "*Ca.* Methylomirabilis oxyfera"
63 which has been suggested to generate intracellular O_2 for CH_4 oxidation from two
64 molecules of NO (Ettwig *et al.* 2010), bacterial methanotrophs couple CH_4 oxidation with
65 free O_2 in the environment. This potential relationship between CH_4 oxidizers (MOs) and
66 electron acceptor availability provides a compelling avenue to explore the response of
67 subsurface communities to natural changes in subsurface fluid chemistry.
68   Our study focuses on the subsurface microbial community of a 1,339 meters-
69 below-land-surface (mbls) fluid-filled fracture (Be326 Bh2). Here, bulk bacterial
70 phospholipid-derived fatty acid (PLFA) isotopic signatures have been shown to be
71 consistent with the accumulation of ^{13}C-dissolved inorganic carbon (DIC) impacted by
72 the microbial oxidation of CH_4 (Simkus *et al.* 2015) but the organisms responsible for
73 CH_4 oxidation have not been well characterized (Magnabosco *et al.* 2014; Simkus *et al.*
74 2015; Young *et al.* 2017). To better describe the membership of native MO communities,
75 their methane oxidizing genes, and their response to changes in fluid chemistry over time,
76 we combined metagenomics, metatranscriptomics, and metaproteomics analyses with
77 geochemical monitoring of Be326 Bh2's *in situ* fracture fluids over both 2.5 year and 2
78 week timescales. We also performed activity assays on the fracture fluids using ^{13}C-
79 labeled CH_4 together with different electron acceptors to track anaerobic methane
80 oxidizing activity in both short- and long-term incubations.
81
82 **Materials and Methods:**
83   Be326 Bh2 was accessed through a 57-m, horizontally drilled borehole that was
84 drilled in 2007 and sealed with a high-pressure steel valve. The borehole is located on the
85 26 level of shaft 3 in the Beatrix Gold Mine (28.232288 S, 26.794365 E; Welkom, South
86 Africa). Annual samples were collected during field trips in 2011, 2012, and 2013 and
87 weekly samples were collected during the 2013 field trip with three time points
88 designated as T_0, T_1, and T_2 with T_0 corresponding to the first day of the 2013 study and
89 T_2 corresponding to the last day of the 2013 study.
90 ***Sampling***
91   Sampling procedures have been outlined previously (Magnabosco *et al.* 2014). To
92 sample, a sterile (combusted and autoclaved) stainless steel manifold with attached valves
93 was attached to the Be326 borehole. A high-pressure steel valve was opened, allowing
94 water to flow freely at ~4-6 L min^{-1} for at least 10 minutes. This manifold allows for the

95   attachment of airtight Teflon tubing and filters for sampling and chemical analysis. For
96   the 2011, 2012, and 2013 samples, pre-autoclaved 0.1-µm Memtrex NY filters (MNY-91-
97   1-AAS; General Electric Co., Minnetonka, MN USA) were left on the borehole for 6, 15,
98   and 14 days, respectively. For the T_0, T_1, and T_2 samples, 0.2-µm Memtrex NY Capsule
99   (CMNY) filters (General Electric Co., Minnetonka, MN USA) were left on the borehole
100   for 2 hours with a flow rate of 500 mL per minute (equivalent to approximately 60 L
101   filtered per time point) in 2013. The total volumes of water filtered for each time point in
102   the 2.5-year study were 4,875 L, 12,604 L, and 6,635 L in 2011, 2012 and 2013,
103   respectively.
104   Unfiltered water samples for direct cell counts were collected on the first day of
105   the 2011, 2012, and 2013 studies and fixed with sterile formaldehyde (final concentration
106   4% v/v). Cell counts were obtained at the University of the Free State where samples
107   were filtered through a sterile 0.22µm Millipore GTTP-type membrane filter, stained
108   with DAPI, and visualized using fluorescence microscopy.

109   ***Geochemical Measurements***
110   Temperature, pH, and E_h were measured at the borehole using handheld probes
111   (HANNA instruments, Woonsocket, RI). Gas samples (H_2, O_2, CH_4) were collected and
112   analyzed by gas chromatography (Peak Performer 1 series, Peak Laboratories, USA)
113   (Simkus *et al.* 2015). Oxygen was also measured at the borehole using a CHEMET kit
114   (Chemetrics Inc.; Calverton, VA). NO_3^- and SO_4^{2-} were measured using an ion
115   chromatograph coupled to an electrospray ionization-quadruple mass spectrometer (MS)
116   (Dionex IC25 and Thermo Scientific MSQ, USA). $\delta^{18}O$ and δ^2H were measured as
117   previously described (Simkus *et al.* 2015).

118   ***Preservation of Biomolecules and extraction***
119   Filters were treated with an RNA preserve solution and stored in a -80°C freezer.
120   The RNA preserve is a custom made solution of 20 mM EDTA, 0.3 M sodium citrate,
121   and 4.3 M ammonium SO_4^{2-} (pH 5.2). The solution was autoclaved prior to sample
122   application. Total protein, together with total DNA and RNA, was extracted using 2X
123   CTAB lysis buffer and phenol/chloroform (pH=6.5-6.9), and re-suspended in 1 TE-buffer
124   (Tris-EDTA, pH = 8) and stored in 1.5-mL Eppendorf tubes at −20°C. Extraction of
125   biomolecules is further described elsewhere (Lau *et al.* 2014, 2016).

126   ***Amplicon Sequencing and Annotation***
127   The V6 region of archaeal 16S rDNA molecules from the 2011 and 2012 time
128   points was amplified using 958F (AATTGGANTCAACGCCGG) and 1048R
129   (CGRCRGCCATGYACCWC) primers. The V4-V5 region of archaeal 16S rDNA
130   molecules from all time points was amplified using the 517F
131   (GCCTAAAGCATCCGTAGC; GCCTAAARCGTYCGTAGC;
132   GTCTAAAGGGTCYGTAGC; GCTTAAAGNGTYCGTAGC;
133   GTCTAAARCGYYCGTAGC) and 958R (CCGGCGTTGANTCCAATT) primers. For
134   both amplicon datasets, forward primers included 5-nt multiplexing barcodes and a
135   reverse 6-nt index. Triplicate PCR amplifications were performed in 33-µL reaction
136   volumes with an amplification cocktail containing 10.0 U Platinum Taq Hi-Fidelity
137   Polymerase (Invitrogen, Carlsbad, CA), 1X Hi-Fidelity buffer, 200 µM dNTP PurePeak
138   DNA polymerase mix (ThermoFisher), 2 mM $MgSO_4$ and 0.3 µM of each primer. We
139   added approximately 10-25 ng template DNA to each PCR and ran a control without
140   template DNA for each primer pair. Amplification conditions were: initial 94°C, 3

141   minute denaturation step; 25 cycles of 94°C for 30 s, 60°C for 45 s, and 72°C for 60 s;
142   and a final 2 minute extension at 72°C. The triplicate PCR reactions were pooled after
143   amplification and purified using Qiagen MinElute plates followed by clean up, PicoGreen
144   quantitation and Sage PippinPrep size selection. 101-nt paired-end sequencing was
145   performed on an Illumina HiSeq 1000 at the Marine Biological Laboratory (Woods Hole,
146   MA USA). Only reads that were identical in the overlapping regions of the forward and
147   reverse reads were included for annotation. In the case of V6 data, this filter necessitates
148   an exact match across both the forward and reverse read. Sequences that met the given
149   quality criteria were annotated using GAST (Huse *et al.* 2008) and a GAST-formatted
150   reference set.

151   *Mapping of Metatranscriptomic Data to V6 Amplicons*
152   Quality filtered RNA reads were mapped to the GAST-annotated V6 amplicons of
153   Be326 Bh2 (Magnabosco *et al.* 2014; Young *et al.* 2017) using BLASTn (percent identity
154   >97%; alignment length > 55 nucleotides (nt)). Reads that mapped positively to V6
155   sequences were assigned a consensus taxonomy based on the top three BLASTn hits.

156   *Generation of Metagenomic and Metatranscriptomic Datasets*
157   DNA samples from 2011 and 2012 were sequenced at the National Center for
158   Genome Resources (Santa Fe, NM). The 2011 and 2012 metagenomic libraries were
159   prepared from 500 ng of DNA using the KAPA High Throughput Library Preparation Kit
160   (KAPA Biosystems), an insert size of approximately 280 bp, and followed by 8 PCR
161   cycles. Paired-end sequencing (2×100 nt) was performed on an Illumina HiSeq 2000.
162   DNA from 2013 was sequenced at Lewis Sigler Institute for Integrative Genomics
163   (Princeton, NJ USA) using an Illumina HiSeq 2500. The metagenomic library was
164   prepared using the TruSeq Rapid SBS Kit, size selected for 380-400 nt, and sequenced
165   using paired-end sequencing (2×215 nt).
166   RNA samples from 2011, 2012, 2013, T_0, T_1, and T_2 were sequenced at Lewis
167   Sigler Institute for Integrative Genomics (Princeton, NJ USA) on an Illumina HiSeq 2500
168   platform. Here, metatranscriptomic libraries were prepared using the Ovation RNA-Seq
169   v2 System (NuGEN; San Carlos, CA USA), which involved 15-18 cycles of PCR. The
170   2011 and 2012 RNA samples were sequenced using 141-nt single-end sequencing while
171   the 2013, T_0, T_1, and T_2 RNA samples were sequenced using 200-nt single-end reads.

172   *Targeted Assembly and Tree Building*
173   Reads were quality filtered and assembled using a targeted assembly pipeline
174   (https://github.com/cmagnabosco/OmicPipelines). In summary, this pipeline involved
175   quality filtering reads using default settings on the fastx toolkit
176   (http://hannonlab.cshl.edu/fastx_toolkit/), targeted assembly of *mcrA* GENEs, protein
177   prediction, alignment of reads to a set of well curated McrA peptides, and the
178   construction of a phylogenic tree from the predicted proteins (PhyML (Guindon *et al.*
179   2010), Best of nearest-neighbor-interchange and subtree-pruning-regrafting, 8 rate
180   categories, -b 100). This procedure was also repeated for the assembly of *mmo* genes
181   using a MMO peptide database.
182   Assembled genes of 200 nt or longer were trimmed to include only the coding
183   region of verified *mcrA* and *mmo* genes. This dataset was used as the reference database
184   (Supplementary Data 2) to map quality-filtered DNA and RNA reads using Bowtie2 (--
185   very-sensitive-local). The coverage was calculated as: (number of reads mapped ×
186   average read length)/length of the reference sequence. For correlation analyses, coverage

187 was normalized by dividing by the total number of reads in the dataset. Pearson
188 correlation coefficients (r) were computed in Excel using the CORREL function.
189 ***Protein Identification from UPLC-MS/MS Data***
190   Ultra performance liquid chromatography-tandem mass spectrometer (UPLC-
191 MS/MS) data were analyzed in aggregate using the SEQUEST HT search engine in
192 ProteomeDiscoverer v1.4 (ThermoFisher Scientific) using a custom database containing
193 the translated genes from the targeted assembly and published McrA, pMoA, MmoX and
194 AmoA (Supplementary Data 4). Search parameters included trypsin digestion with up to
195 one missed cleavage, methionine oxidation and cysteine carbamidomethylation. A
196 peptide-level false discovery rate (FDR) of 5% was achieved by using the Percolator
197 node in ProteomeDiscoverer, which utilizes the frequency of matching against a reversed
198 database as a rigorous model of the probability of error in the forward matches at given
199 score thresholds. Proteins identified by matches to one unique peptide per run were
200 tallied.
201 *Activity assays*
202   During the 2012 and 2013 sampling points, water samples were collected into
203 150-mL serum vials ("biovials") and stored at 4°C. Two days prior to sampling, 100 µL
204 of MilliQ water was added to a 150-mL serum vial that had undergone combustion in an
205 oven at 450°C overnight to deactivate spores. The serum vial was then sealed with a
206 butyl rubber stopper that was cleaned by boiling in 0.1 M NaOH solution for 1 hour,
207 rinsed and left to soak in MilliQ water until use. The serum vials were then crimped and
208 left overnight. The next day, the serum vials were purged and pressurized with filtered
209 N_2. The vials were then autoclaved and bubble-wrapped for transport underground. A
210 needle was attached to the end of sterile teflon tubing that was attached to the manifold.
211 Water was allowed to flow to rinse the attachment and needle. After 2 minutes of rinsing,
212 the needle was inserted into the biovial and a second needle was added for pressure relief.
213 Water was allowed to flow into the biovial until the relief needle overflowed. Extensive
214 care was taken to ensure that no visible gas bubble remained in the biovial post-sampling.
215   Two sets of enrichment experiments were performed to monitor the response of
216 the biovial communities to methane and a variety of electron acceptors. Experiment 1
217 contained samples from 2012 and 2013. Samples were incubated in triplicate with ^{13}C-
218 CH_4 and SO_4^{2-} (20 mM) or ^{13}C-CH_4 and NO_3^- (20 mM) for 207 and 185 days,
219 respectively. A control incubation with ^{13}C-CH_4 and no electron acceptors was monitored
220 for 207 days to measure endogenous $^{13}CO_2$ production (Control A). Experiment 2
221 included samples from 2012 and 2013 that were incubated in triplicate with ^{13}C-CH_4 and
222 SO_4^{2-} (20 mM), NO_3^- (20 mM) or O_2 (5% v/v). A killed (paraformaldehyde, 4% v/v)
223 control without electron acceptors (Control 1) and a live control without electron acceptor
224 or donor were included (Control 2). All samples of Experiment 2 were incubated and
225 monitored over a 43-day period.
226   The samples for all experiments were prepared in 14-mL serum vials sealed with
227 butyl rubber stoppers and aluminum caps. Prior to sample addition, vials were made
228 anoxic by exchanging headspace gas with N_2 for 10 cycles and left pressurized (0.5 bar
229 overpressure). 10 mL aliquots of fracture fluid were then added to the vials in an anoxic
230 chamber and amended with the treatments described above. When ^{13}C-CH_4 was added,
231 N_2 was added to a pressure of 130 kPa and 99.99% ^{13}C-CH_4 gas (Campro Scientific,
232 Veenendaal, The Netherlands) was added to a final pressure of 180 kPa. Oxygen was

233   added afterwards, when applicable. All electron acceptor solutions were sterile and
234   anoxic. The serum bottles were statically incubated at 37°C in the dark.
235   NO_3^- and SO_4^{2-} were analysed using an ion chromatography system equipped with
236   an Ionpac AS9-SC column and an ED 40 electrochemical detector (Dionex, Sunnyvale,
237   CA). The system was operated at a column temperature of 35°C, and a flow rate of 1.2 ml
238   min^{-1}. Eluent consisted of a carbonate/bicarbonate solution (1.8 and 1.7 mM respectively)
239   in deionized water. Headspace gas composition was measured on a gas chromatograph-
240   mass spectrometer (GC-MS) composed of a Trace GC Ultra (Thermo Fisher Scientific,
241   Waltham, MA) equipped with a Rt-QPLOT column (Restek, Bellefonte, PA), and a DSQ
242   MS (Thermo Fisher Scientific). Helium was used as a carrier gas with a flow rate of 120
243   ml min^{-1} and a split ratio of 60. The inlet temperature was 80°C; the column temperature
244   was set at 40°C and the ion source temperature was 200°C. CH_4 and CO_2 in the
245   headspace were quantified from the peak areas in the gas chromatographs. The fractions
246   of $^{13}CO_2$, $^{13}CH_4$ and $^{12}CH_4$ were derived from the mass spectrum (Shigematsu *et al.*
247   2004). Validation of the method was done using standards with known mixture of $^{13}CO_2$
248   and $^{12}CO_2$. The concentrations of total CO_2, total CH_4, and $^{13}CO_2$ were calculated
249   following the method of Timmers *et al.* (2015). The pressure of the serum vials was
250   determined using a portable membrane pressure unit (GMH 3150, Greisinger electronic
251   GmbH, Regenstauf, Germany). The pH was checked by a standard pH electrode (QiS,
252   Oosterhout, The Netherlands).
253
254   **Results and Discussion:**
255   *A changing fluid chemistry over time*
256   Over a period of 2.5 years, water isotope analysis revealed large changes in the
257   fracture fluid's δ^2H and $\delta^{18}O$ isotopic signatures (Fig. 1; purple squares). These changes
258   are inconsistent with contamination with service water in the mine and, instead, indicate
259   mixing of different fracture waters within the system. In 2011, the $\delta^{18}O$ and δ^2H values
260   were on the global meteoric water line (GMWL) and are indicative of paleometeoric
261   water. This isotopic signature is consistent with other fluids located approximately 1,000
262   to 1,500 mbls in the Witwatersrand Formation (South Africa) (Fig. 1; green triangles)
263   (Onstott *et al.* 2006; Sherwood Lollar *et al.* 2007). In 2012 and 2013, the $\delta^{18}O$ and δ^2H
264   signatures of the fluids moved away from the GMWL, indicating mixing with more
265   ancient fluids (Frape *et al.* 1984). A few meters away, Be326 Bh1 (a borehole located in
266   the same mine and depth as the Be326 borehole of this study) exhibited a similar trend in
267     $\delta^{18}O$ and δ^2H signatures over time—shifting away from the GMWL in 2012 and 2013
268   (Fig. 1; red diamonds). The displacements between the 2011/2012 and 2012/2013 $\delta^{18}O$
269   and δ^2H signatures of the two boreholes are in opposite directions—a pattern that would
270   not be expected if the native fracture fluids were mixing with the mine's service water
271   during this period. Measurements of the fracture fluid's δ^2H and $\delta^{18}O$ isotopic signatures
272   over the 2-week study were not obtained.
273   Geophysico-chemical measurements were made for both the 2.5-year and 2-week
274   time series (Table 1). Temperature, pH, and CH_4 concentrations were relatively
275   unchanged in both of the time series but the degree to which E_h, SO_4^{2-}, NO_3^-, and H_2
276   concentrations changed was much greater over the 2.5 years (Table 1a). Within the 2.5-
277   year time series, the fracture fluids shifted from a more reduced state (2011_{Eh} = -98 mV,
278     $2011_{[H2]}$ = 130 nM) with limited electron acceptor availability ($2011_{[Sulph.]}$ = 137μM,

279    $2011_{[Nitr.]} = 0.4$ µM) to a more oxidized state ($2013_{Eh} = 21\pm28$ mV, $2013_{[H2]} = 25$ nM)

280   with much greater electron acceptor availability ($2013_{[Sulph.]} = 479$ µM, $2013_{[Nitr.]} = 4.5$

281   µM). The 2-week time series did not exhibit as large of a shift in electron acceptor

282   availability as the 2.5-year time series and maintained a positive E_h throughout (Table

283   1b).

284   *Microbial community of Be326*

285   The microbial communities of the 2011 and 2012 time points have been reported

286   to be dominated by bacteria (98.5%) (Simkus *et al.* 2015) with the majority being related

287   to Proteobacteria (Magnabosco *et al.* 2014). In order to investigate the community

288   composition of the less numerous archaea, 16S rDNA amplicon sequencing of the

289   archaeal V4-V5 hypervariable region was performed across all time points (Fig. 2a). For

290   the long-term study (2011, 2012, 2013), the archaeal community shifted from an ANME-

291   1- and Methanomicrobia-dominated community in 2011 to a Miscellaneous

292   Crenarchaeotic Group-dominated community in 2012 and a Halobacteria-dominated

293   community in 2013. For the short-term study (T_0, T_1, T_2), there were no noticeable

294   changes between T_1 and T_2. A slight increase in Halobacteria and a decrease in ANME-1

295   with respect to T_1 and T_2 were observed in the T_0 time point. There is a noticeable

296   difference between the T_0, T_1, T_2 samples community profiles and the 2013 community

297   profile, despite being collected over the same two-week period. However, the filters used

298   in the T_x and 2013 filtrations have varied pore sizes, geometries, and casings and should

299   not be directly compared.

300   Around 1% of V4-V5 amplicons were related to "*Ca.* M. nitroreducens" in all

301   time points except for the 2011 dataset that contained only 2 archaeal amplicons relating

302   to "*Ca.* M. nitroreducens" (Supplementary Data 1). These relative abundances of "*Ca.* M.

303   nitroreducens" are lower than what was reported using archaeal V6 primers on 2011 and

304   2012 samples. With archaeal V6 primers, "*Ca.* M. nitroreducens" accounts for 1.5% of

305   the archaeal community in 2011 and 10.6% of the archaeal community in 2012, while

306   ANME-1 accounts for ~10% of the archaeal community at each time point (Young *et al.*,

307   2017; Supplementary Fig. S1). Despite differences in the relative abundances of taxa

308   based on the primers used, community membership does not appear to be significantly

309   different between the 2 primer sets.

310   In order to estimate the relative activity of each taxonomic group,

311   metatranscriptomic data from each sample were mapped to a database of Be326 Bh2 16S

312   rDNA V6 bacterial (Magnabosco *et al.* 2014) and archaeal (Young *et al.* 2017)

313   sequences. The V6 sequences were selected over the V4-V5 sequences due to their

314   shorter length and stringent quality filtering procedure (see Materials & Methods).

315   Proteobacteria within the family Rhodocyclaceae dominated all of the RNA datasets

316   except for the 2011 dataset that was dominated by Hydrogenophilaceae. The number of

317   bacterial and archaeal species (unique hits within the 16S rDNA V6 database) observed

318   in the metatransciptomic data ranged from 204 in 2013's T_0 time point to 414 in the 2012

319   sample (Table 2). MO archaea and bacteria account for only a small percentage of the V6

320   rRNA sequences identified in the metatranscriptomic data (0.3-3%). Notably, the number

321   of species observed in each metatranscriptome's V6 rRNA pool was not correlated to the

322   number of reads generated for each metatranscriptome ($R^2 < 0.01$); however, the number

323   of species observed in each metatranscriptome is almost 10 times less than the number of

324 OTU$_{0.97}$ obtained from the bacterial 16S rDNA V6 dataset (2,478 in 2011 and 3,987 in
325 2012) (Magnabosco *et al.* 2014).

A detectable shift in the MO community over time

327 As the organisms responsible for CH$_4$ oxidation in Be326 were present at
328 relatively low abundances, a targeted assembly pipeline
329 (https://github.com/cmagnabosco/OmicPipelines) that employs the PRICE assembler
330 (Ruby, Bellare and DeRisi 2013) was implemented to assemble methyl-coenzyme M
331 reductase (*mcrA*)—the gene for the first step in the anaerobic oxidation of methane
332 (AOM) (Thauer 2011) or the last step in methanogenesis—and a suite of CH$_4$
333 monooxygenases (*mmo*) that are known to play a role in aerobic oxidation of methane
334 (McDonald *et al.* 2008) from the metagenomic and metratranscriptomic datasets.
335 Notably, *mcrA* was selected as an indicator for ANME presence because its phylogeny is
336 congruent with MO phylogeny.

337 Following targeted assembly and annotation, two complete *mcrA* genes related to
338 ANME-1 and "*Ca.* M. nitroreducens", an ANME-2d, were assembled. Only one
339 complete *mmo* gene closely related to *Methylococcus capsulatus* was recovered from the
340 metagenomic and metatranscriptomic data (Fig. 2b, Supplementary Data 2). Partial *mcrA*
341 related to Methanomicrobia and Methanobacteria were also identified in the high-
342 throughput data (Fig. 2b, Supplementary Data 2), but partially assembled *mmo*-related
343 genes were omitted in downstream analyses due to the difficulty in distinguishing *mmo*
344 from homologous ammonia monooxygenases genes (Holmes *et al.* 1995).

345 Assembled *mcrA* and *mmo* were translated into peptide sequences
346 (Supplementary Data 3). Notably, the Be326 "*Ca.* M. nitroreducens"-type McrA was
347 99% identical to the McrA of the reference "*Ca.* M. nitroreducens" genome
348 (Supplementary Data 3, 4). Metaproteomic data were searched against the collection of
349 assembled McrA and MMO and a database of known McrA and MMO peptide sequences
350 (Supplementary Data 4) to confirm that the transcribed genes were translated into
351 proteins. The predicted amino acid sequences (Supplementary Data 3) from the
352 assembled ANME-1, "*Ca.* M. nitroreducens", and *Methylococcus* genes were all
353 identified within the metaproteomic data (Fig. 3, Supplementary Data 5) which further
354 confirmed the presence and activity of these groups of organisms.

355 The abundances (based on coverage) of each MO gene (*mcr,A mmo*) and MO 16S
356 SSU rRNA gene were calculated using Bowtie2 (Langmead and Salzberg 2012) (-very-
357 sensitive-local) and BLASTn, respectively. These analyses provided evidence that the
358 dominant members of the MO community in the metagenomes and metatranscriptomes
359 shifted from ANME-1 to "*Ca.* M. nitroreducens" during the 2.5-year sampling period
360 (Fig. 2) but remained constant during the 2-week sampling period (Supplementary Table
361 1). These observations were consistent with the relative changes in geochemistry over
362 both time scales (Table 1). Notably, "*Ca.* M. nitroreducens" accounted for ≤1% of the
363 archaeal community, as revealed using archaeal V4-V5 16S rDNA primers (Fig. 1),
364 which is in contrast to the higher estimates of "*Ca.* M. nitroreducens" found when using
365 archaeal V6 16S rDNA (Young *et al.*, 2017; Supplementary Fig. S1), metagenomic and
366 metatranscriptomic data. This discrepancy suggests that "*Ca.* M. nitroreducens"
367 sequences are recovered at a lower efficiency in archaeal V4-V5 16S SSU rRNA gene
368 surveys relative to archaeal V6 16S SSU rRNA gene surveys, metagenomic and
369 metatranscriptomic studies.

When metagenomic MO *mcrA* and *mmo* abundances of the long-term study (Supplementary Table 2) were correlated to geophysico-chemical measurements, "*Ca.* M. nitroreducens" was positively correlated to NO_3^- (R^2=0.99) and SO_4^{2-} (R^2=0.98) concentrations but negatively correlated to CH_4 (R^2=0.99) and H_2 (R^2=0.99) concentrations. ANME-1 *mcrA* abundances showed an opposite trend and were positively correlated to CH_4 (R^2=0.96) and H_2 (R^2=0.97) concentrations but negatively correlated NO_3^- (R^2=0.88) and SO_4^{2-} (R^2=0.85) concentrations (Table 3). Correlation of metatranscriptomic 16S rRNA and *mcrA* and *mmo* abundances to geophysico-chemical measurements exhibited similar trends (Supplementary Table 3) and are consistent with a transition from an ANME-1-dominated MO community to a "*Ca.* M. nitroreducens"-dominated community. As NO_3^--coupled CH_4 oxidation is more energetic than SO_4^{2-}-coupled CH_4 oxidation (Caldwell *et al.* 2008), an energetic advantage, presumably, provides "*Ca.* M. nitroreducens" a competitive advantage against ANME-1 when NO_3^- concentrations are sufficient.

O_2 concentrations in 2011 and 2013 were below detection limit (Table 1) but were detectable in 2012 (0.47 μM). Likely related to the increased availability of O_2, aerobic *Methylococcus*-related *mmo* genes exhibited their highest relative abundances within metagenomic and metatranscriptomic MO gene profiles during 2012 and a minimal presence throughout the remainder of the time points (Fig. 2, Supplementary Table 1). "*Ca.* M. nitroreducens" was the dominant member (73.2±2.8%) of the MOs community during the 2-week time series (Supplementary Table 1) when fracture fluids contained high concentrations of SO_4^{2-} (496±36 μM) and NO_3^- (4.8±0.9 μM) along with a positive E_h (21±28 mV).

The correlations between MO abundances and fluid chemistry suggest that a relationship between electron acceptor availability and populations of MOs exists. We therefore wanted to experimentally validate the response of the MOs to changes in electron acceptor availability. As ANME-1, "*Ca.* M. nitroreducens", and *Methylococcus* are best described as a SO_4^{2-}-dependent ANME (Wegener *et al.* 2015), NO_3^--dependent ANME (Haroon *et al.* 2013), and aerobic methanotrophs (Kleiveland *et al.* 2012), respectively, we designed experiments to test whether or not each MO lifestyle would respond to an increase in the aforementioned electron acceptor.

Validation of the MO community through $^{13}CH_4$ enrichments

To better understand the response of the MO community to changes in electron donor/acceptor balance, two sets of ^{13}C-CH_4 laboratory enrichment experiments were performed on fracture water collected in 2012 and 2013. The first experiment (Experiment 1) was a long-term experiment analyzed over 207[*] days and contained fracture fluid samples from 2012 and 2013 enriched with either ^{13}C-CH_4 and no additional electron acceptor (endogenous activity control), ^{13}C-CH_4+SO_4^{2-} (to stimulate SO_4^{2-}-dependent AOM), or ^{13}C-CH_4+NO_3^- (to stimulate NO_3^--dependent AOM). A second set of 2012 and 2013 fracture fluid enrichments (Experiment 2) was analyzed for 43 days. Experiment 2 contained ^{13}C-CH_4 treatments of ^{13}C-CH_4+formaldehyde (4%, v/v) (killed control) to rule out non-biological sources of ^{13}C-CH_4 production, ^{13}C-CH_4+SO_4^{2-}, ^{13}C-CH_4+O_2 (to simulate aerobic methane oxidation), and ^{13}C-CH_4+NO_3^- as well as an electron acceptor- and donor-free control (methanogenesis control). The

---

[*] The long term ^{13}C-CH_4+NO_3^- enrichments were run for 183 days.

9

414 methanogenesis control was intended to detect whether or not methanogenesis, and
415 therefore also trace CH_4 oxidation (TMO),was occurring within the samples (Zehnder
416 and Brock 1979). Due to the limited amount of sample, we were unable to test the
417 potential occurrence of Mn^{4+}-or Fe^{3+}-driven methane oxidation.
418   Unlike the correlations observed between expression data and geochemical
419 parameters, an increase in the proportion of ^{13}C-CO_2 relative to total CO_2 ($\%^{13}C$-CO_2) in
420 the $^{13}CH_4$ enrichments over time provides definitive evidence of $^{13}CH_4$ oxidation under
421 different conditions. Notably, we chose to express our results as $\%^{13}C$-CO_2 rather than
422 the absolute concentration (molar) of ^{13}C-CO_2 to account for CO_2 production from other
423 substrates. In Experiment 1, the ^{13}C-CH_4+NO_3^- enrichments exhibited the greatest rate of
424 $\%^{13}C$-CO_2 production and, in 2012, the rate of $\%^{13}C$-CO_2 production (0.017 ± 0.005 $\%^{13}C$-
425 CO_2 day^{-1}) was found to be significantly greater (paired one-tailed Student t-test; p=0.02)
426 than in Control A (0.004 ± 0.001 $\%^{13}C$-CO_2 day^{-1}) (Fig. 4). No samples from Experiment
427 2 exhibited an increase in $\%^{13}C$-CO_2 production (Supplementary Data 5).
428   Although ANME-1 were present in the metatranscriptomic and metaproteomic
429 data during the 2012 and 2013 sampling points, there was not a significant difference in
430 $\%^{13}C$-CO_2 production between Experiment 1's ^{13}C-CH_4+SO_4^{2-} incubations and the
431 endogenous activity controls (Fig. 4). TMO was probably not responsible for the ^{13}C-CO_2
432 production in the endogenous activity controls of Experiment 1; only the methanogenesis
433 control of the 2013 sample showed minor methanogenesis (and thus TMO) activity
434 (Supplementary Data 5). It is conceivable, however, that SO_4^{2-}-dependent AOM occurred
435 in both the endogenous controls and ^{13}C-CH_4+SO_4^{2-} incubations, as the concentrations of
436 SO_4^{2-} in the controls ([$SO_4^{2-}{}_{2012}$] = 623 μM; [$SO_4^{2-}{}_{2013}$] = 479 μM) are well within the
437 lower range of SO_4^{2-} concentrations (100-1200 μM) that have been reported for SO_4^{2-}-
438 coupled AOM (Beal, Claire and House 2011; Segarra *et al.* 2015). Combined, these
439 findings suggest that SO_4^{2-}-coupled AOM likely occurred in the controls of Experiment 1
440 and 2.
441
442 **Conclusions:**
443   Metagenomic, metatranscriptomic, and metaproteomic data suggest that
444 community composition, activity, and function are changing in response to natural
445 fluctuations in fluid chemistry. The observed CH_4 oxidation in the controls and
446 dominance of ANME-1 in the 2011 samples (when SO_4^{2-} concentrations were lowest)
447 indicate that the *in situ* fluids contain enough SO_4^{2-} to power SO_4^{2-}-coupled MO. The
448 increase in $\%^{13}C$-CO_2 production in the ^{13}C-CH_4+NO_3^- enrichments and correlation of
449 "*Ca.* Methanoperedens" abundances to electron acceptor concentrations *in situ* suggest
450 that electron acceptor availability plays an important role in MO population dynamics.
451 Together, these results provide the most conclusive biological evidence to date that CH_4
452 oxidation occurs and is an integral component of the deep terrestrial subsurface carbon
453 cycle.
454
455 **Data Availability:**
456 Metagenomic and metatranscriptomic data are available at NCBI BioProject
457 PRJNA308990. 16S amplicon data are available under NCBI BioProject PRJNA263371.
458
459

460 **Tables and Figures:**

461

462 **TABLE 1a. Geophysico-chemical measurements for the long-term study**

463

	2011	**2012**	**2013**
Dates Sampled	Jan 21-27, 2011	July 12-27, 2012	Aug 1-15, 2013
Temperature (°C)	36.9	37.3±1.2	35.1±0.8
pH	8.83	8.55	8.17±0.7
E_h (mV)	-98	-27.5±6.4	21±28
SO_4^{2-} (µM)	137	623	479
NO_3^- (µM)	0.4	6.0	4.5
O_2 (Chemet) (µM)	b.d.	0.47	b.d.*
H_2 (nM)	130	9	25
CH_4 (mM)	2.0	0.9	1.1

464

465 b.d. = below detection (<0.31 µM)

466 b.d.* = below detection (<1.6 µM)

467

468 **Table 1b. Geophysico-chemical measurements for the short-term study**

469

	T_0	**T_1**	**T_2**
Dates Sampled	Aug 1, 2013	Aug 8, 2013	Aug 15, 2013
Temperature (°C)	35.8	35.3	28.6
pH	8.2	8.1	7.9
E_h (mV)	9	53	1
SO_4^{2-} (µM)	531	499	459
NO_3^- (µM)	5.3	5.3	3.7
O_2 (Chemet) (µM)	b.d.*	b.d.*	b.d.*
H_2 (nM)	5.8×10^{-5}	10.4	39.8
CH_4 (mM)	0.8	1.2	1.0

470 b.d.* = below detection (<1.6 µM)

471

472

473

474

475

476

477

478

479

480

481

482

483

484

Table 2: Metatranscriptomic species richness observed and estimated by Chao 1 and ACE metrics and cell concentrations measured in the field.

	2011	2012	2013	T_0	T_1	T_2
Species (S) Observed	302	414	247	222	204	248
S.Chao1	344±22	440±10	256±7	233±9	216±8	276±16
S.ACE	317±8	450±10	253±6	233±5	212±7	260±8
Cell concentration ($\times 10^3$ cells mL^{-1})	1.3^- 18.3*	2.2*- 31^	3.2^	3.2^	n.m.	n.m.

^DAPI-derived cell concentration

*PLFA-derived cell concentration using a conversion factor of 6×10^4 cells/pmol PLFA as previously reported in Simkus et al. (2015)

n.m. = not measured

Table 3: Correlation (R^2) between normalized metagenomic *mcrA* or *mmo* PEG coverage and geochemical parameters. Positive correlations are underlined.

		NO_3^-	SO_4^{2-}	CH_4	E_h	pH	H_2
2.5-Year Time Series	"*Ca.* Methanoperedens"	<u>0.99</u>	<u>0.98</u>	0.99	<u>0.70</u>	0.52	0.99
	ANME-1	0.88	0.85	<u>0.93</u>	0.90	<u>0.76</u>	<u>0.95</u>
	Methylococcales	<u>0.12</u>	<u>0.14</u>	0.07	0.10	<u>0.25</u>	0.05

507   **Figure 1. δ^2H_{H2O} and $\delta^{18}O_{H2O}$ for Beatrix (Be) Gold Mine fracture fluids.**

508   This figure plots the $\delta^{18}O$ (x-axis) against the δ^2H (y-axis) for each of the three time

509   points (purple squares) in the long-term study of Be326 (2011, 2012, 2013). The black

510   diagonal line represents the global meteoric water line (Craig 1961) (GMWL). The 2011

511   sample sits on the GMWL, consistent with historic Be datapoints (green triangles) and

512   paleometeoric water (Lippmann *et al.* 2003; Ward *et al.* 2004). The 2012 and 2013 time

513   points are displaced away from the GMWL along trends that have been observed to be

514   consistent with mixing with older, more saline fracture fluids (Ward *et al.* 2004;

515   Sherwood Lollar *et al.* 2007). The dotted blue lines indicate possible mixing patterns.

516   Be326_Bh1 (red diamonds) is a borehole located in the same mine and at the same depth

517   as the borehole sampled in this study. EV=Evander Mine; KL=Kloof. Data for EV, KL,

518   and Adams are adapted from Ward *et al.* (2004).
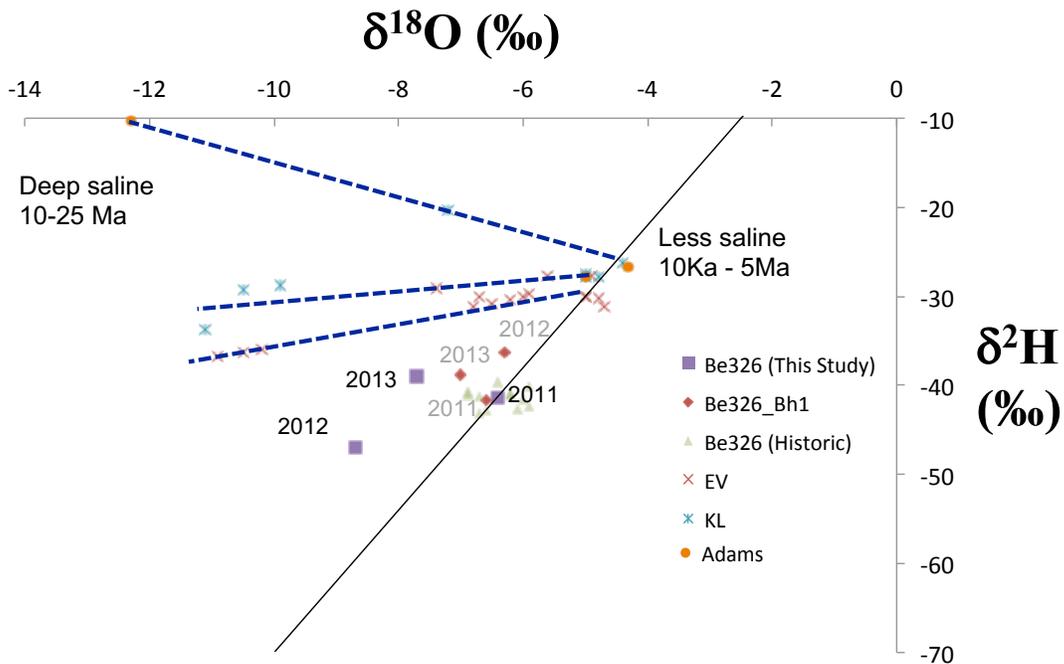
519
520
521
522
523
524
525
526
527
528
529
530

Figure 2. Change in the CH$_4$ oxidizing community and activity over time.

a) The relative abundance (bar height) of major archaeal groups (colors of bars) identified in the archaeal V4-V5 16S rDNA surveys are shown. b) A phylogenetic tree was constructed using PhyML from a McrA peptide database (Supplementary Data 6) and the predicted proteins from the *mcrA* targeted assembly (designated by a *). The predicted MMO from the targeted assembly is also displayed. The 2×3 blocks represent the relative abundance of each taxon (DNA, left column; RNA, right column) with respect to their CH$_4$-related protein of interest (McrA or MMO) over time (row 1, 2011; row 2, 2012; row 3; 2013). Notably, Methanobacteria-related McrA PEGs were selected as the outgroup in this presentation of the McrA phylogenetic tree due to Methanobacteria's placement in species tree of Euryarchaeota.

Figure 3: Peptide mapping to identified McrA and MMO proteins

557
558
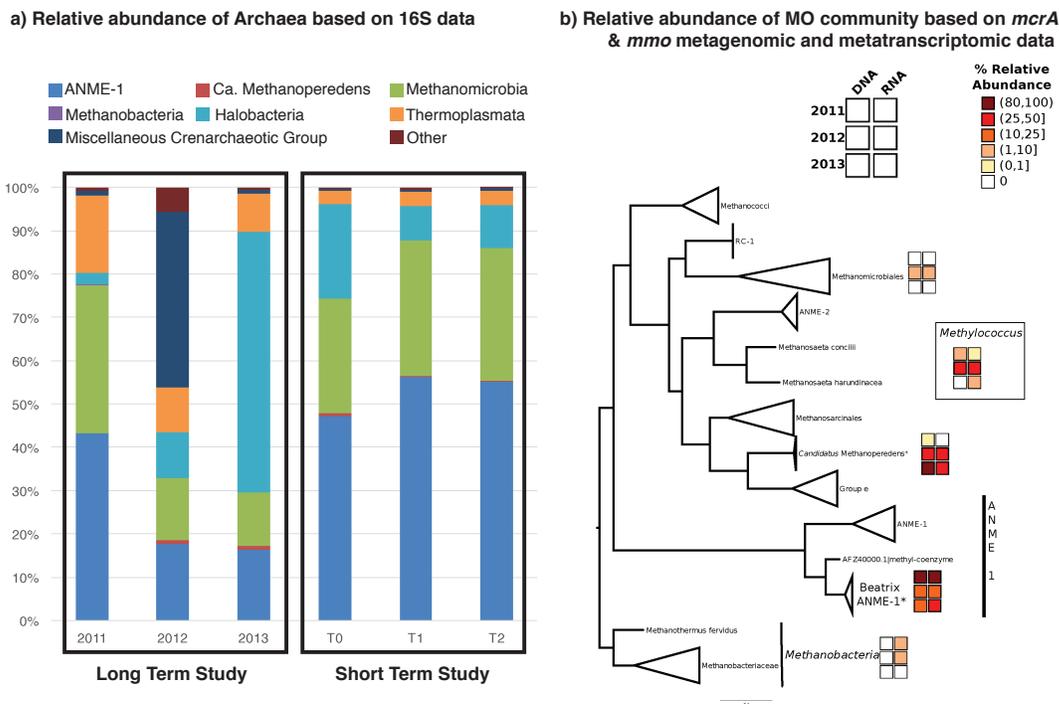
559 **Figure 4: ^{13}C-CO$_2$ production after ^{13}C-CH$_4$ enrichment.**
560 The rates of ^{13}C-CO$_2$ production ($\%^{13}$C-CO$_2$ day^{-1}) from the 2012 (gray) and 2013 (black)
561 fluids of Experiment 1 are displayed. The 2012 samples were run in triplicate and the
562 standard deviations are shown. The star above the 2012 CH4+NO3 bar indicates that the
563 rate of ^{13}C-CO$_2$ production in the ^{13}C-CH4+NO$_3^-$ enrichment was significantly greater
564 (p=0.02) than the electron acceptor-free control (Control A).
565
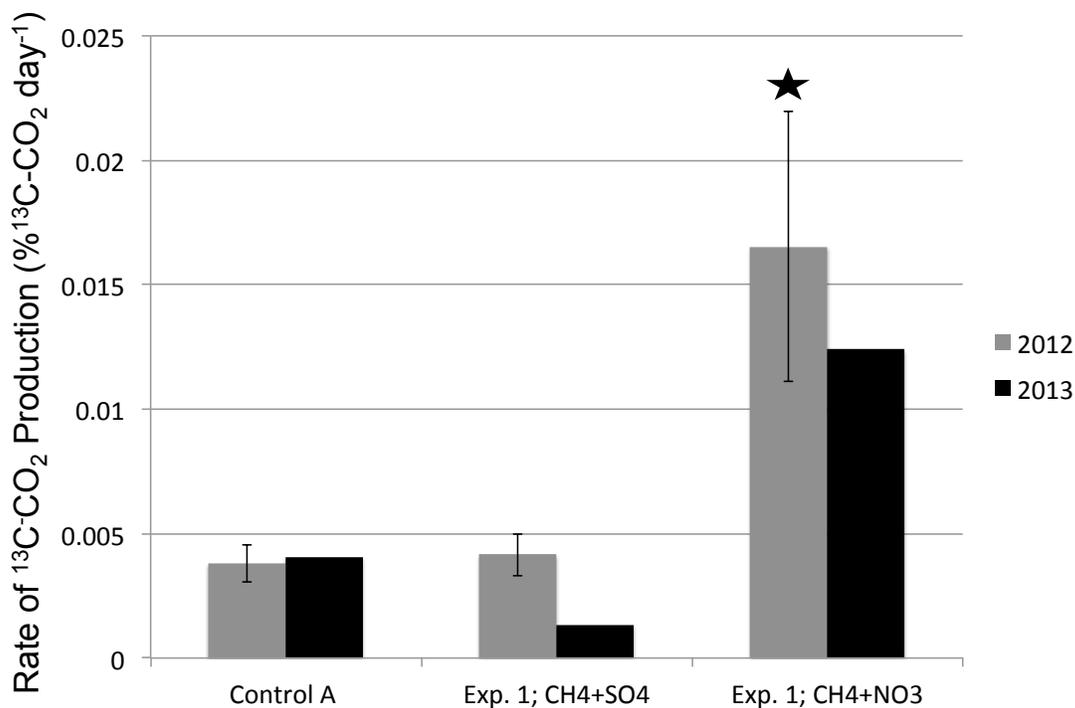
566
567
568
569
570
571
572
573
574
575
576
577
578
579
580
581
582
583
584

615 **References**

616 Bagnoud A, Chourey K, Hettich RL *et al*. Reconstructing a hydrogen-driven microbial
617   metabolic network in Opalinus Clay rock. *Nat Commun* 2016;**7**.

618 Beal EJ, Claire MW, House CH. High rates of anaerobic methanotrophy at low sulfate
619   concentrations with implications for past and present methane levels. *Geobiol*
620   2011;**9**:131–9.

621 Caldwell SL, Laidler JR, Brewer EA *et al*. Anaerobic oxidation of methane: mechanisms,
622   bioenergetics, and the ecology of associated microorganisms. *Environ Sci Technol*
623   2008;**42**:6791–9.

624 Daly RA, Borton MA, Wilkins MJ *et al*. Microbial metabolisms in a 2.5-km-deep
625   ecosystem created by hydraulic fracturing in shales. *Nat Microbiol* 2016;**1**:16146.

626 Ettwig KF, Butler MK, Le Paslier D *et al*. Nitrite-driven anaerobic methane oxidation by
627   oxygenic bacteria. *Nature* 2010;**464**:543–8.

628 Ettwig KF, Zhu B, Speth D *et al*. Archaea catalyze iron-dependent anaerobic oxidation of

629   methane. *Proc Natl Acad Sci* 2016;**113**:12792–6.

630   Frape SK, Fritz P, McNutt RH t. Water-rock interaction and chemistry of groundwaters
631   from the Canadian Shield. *Geochim Cosmochim Acta* 1984;**48**:1617–27.

632   Guindon S, Dufayard J-F, Lefort V *et al*. New algorithms and methods to estimate
633   maximum-likelihood phylogenies: assessing the performance of PhyML 3.0. *Syst*
634   *Biol* 2010;**59**:307–21.

635   Haroon MF, Hu S, Shi Y *et al*. Anaerobic oxidation of methane coupled to nitrate
636   reduction in a novel archaeal lineage. *Nature* 2013;**500**:567–70.

637   Holmes AJ, Costello A, Lidstrom ME *et al*. Evidence that participate methane
638   monooxygenase and ammonia monooxygenase may be evolutionarily related. *FEMS*
639   *Microbiol Lett* 1995;**132**:203–8.

640   Huse SM, Dethlefsen L, Huber JA *et al*. Exploring microbial diversity and taxonomy
641   using SSU rRNA hypervariable tag sequencing. *PLoS Genet* 2008;**4**, DOI:
642   10.1371/journal.pgen.1000255.

643   Kleiveland CR, Hult LTO, Kuczkowska K *et al*. Draft genome sequence of the methane-
644   oxidizing bacterium Methylococcus capsulatus (Texas). *J Bacteriol* 2012;**194**:6626.

645   Langmead B, Salzberg SL. Fast gapped-read alignment with Bowtie 2. *Nat Methods*
646   2012;**9**:357–9.

647   Lau MCY, Cameron C, Magnabosco C *et al*. Phylogeny and phylogeography of
648   functional genes shared among seven terrestrial subsurface metagenomes reveal N-
649   cycling and microbial evolutionary relationships. *Front Microbiol* 2014;**5**.

650   Lau MCY, Kieft TL, Kuloyo O *et al*. An oligotrophic deep-subsurface community
651   dependent on syntrophy is dominated by sulfur-driven autotrophic denitrifiers. *Proc*
652   *Natl Acad Sci* 2016:201612244.

653   Magnabosco C, Tekere M, Lau MCY *et al*. Comparisons of the composition and
654   biogeographic distribution of the bacterial communities occupying South African
655   thermal springs with those inhabiting deep subsurface fracture water. *Front*
656   *Microbiol* 2014;**5**:679.

657   McDonald IR, Bodrossy L, Chen Y *et al*. Molecular ecology techniques for the study of
658   aerobic methanotrophs. *Appl Environ Microbiol* 2008;**74**:1305–15.

659   Morozova D, Wandrey M, Alawi M *et al*. Monitoring of the microbial community
660   composition in saline aquifers during CO_2 storage by fluorescence in situ
661   hybridisation. *Int J Greenh Gas Control* 2010;**4**:981–9.

662   Morozova D, Zettlitzer M, Let D *et al*. Monitoring of the microbial community
663   composition in deep subsurface saline aquifers during CO_2 storage in Ketzin,
664   Germany. *Energy Procedia* 2011;**4**:4362–70.

665   Onstott TC, Lin L-H, Davidson M *et al*. The origin and age of biogeochemical trends in
666   deep fracture water of the Witwatersrand Basin, South Africa. *Geomicrobiol J*
667   2006;**23**:369–414.

668   Purkamo L, Bomberg M, Nyyssönen M *et al*. Dissecting the deep biosphere: retrieving
669   authentic microbial communities from packer-isolated deep crystalline bedrock

670   fracture zones. *FEMS Microbiol Ecol* 2013;**85**:324–37.

671   Rajala P, Bomberg M, Kietäväinen R *et al*. Rapid reactivation of deep subsurface
672   microbes in the presence of C-1 compounds. *Microorganisms* 2015;**3**:17–33.

673   Ruby JG, Bellare P, DeRisi JL. PRICE: software for the targeted assembly of
674   components of (meta) genomic sequence data. *G3 Genes/ Genomes/ Genet*
675   2013;**3**:865–80.

676   Segarra KEA, Schubotz F, Samarkin V *et al*. High rates of anaerobic methane oxidation
677   in freshwater wetlands reduce potential atmospheric methane emissions. *Nat*
678   *Commun* 2015;**6**.

679   Sherwood Lollar B, Voglesonger K, Lin L-H *et al*. Hydrogeologic controls on episodic
680   H2 release from Precambrian fractured rocks-Energy for deep subsurface life on
681   Earth and Mars. *Astrobiology* 2007;**7**:971–86.

682   Shigematsu T, Tang Y, Kobayashi T *et al*. Effect of dilution rate on metabolic pathway
683   shift between aceticlastic and nonaceticlastic methanogenesis in chemostat
684   cultivation. *Appl Environ Microbiol* 2004;**70**:4048–52.

685   Simkus DN, Slater GF, Lollar BS *et al*. Variations in microbial carbon sources and
686   cycling in the deep continental subsurface. *Geochim Cosmochim Acta* 2015.

687   Thauer RK. Anaerobic oxidation of methane with sulfate: on the reversibility of the
688   reactions that are catalyzed by enzymes also involved in methanogenesis from CO 2.
689   *Curr Opin Microbiol* 2011;**14**:292–9.

690   Timmers PHA, Gieteling J, Widjaja-Greefkes HCA *et al*. Growth of anaerobic methane-
691   oxidizing archaea and sulfate-reducing bacteria in a high-pressure membrane
692   capsule bioreactor. *Appl Environ Microbiol* 2015;**81**:1286–96.

693   Wegener G, Krukenberg V, Riedel D *et al*. Intercellular wiring enables electron transfer
694   between methanotrophic archaea and bacteria. *Nature* 2015;**526**:587–90.

695   Young ED, Kohl IE, Lollar BS *et al*. The relative abundances of resolved l2 CH 2 D 2
696   and 13 CH 3 D and mechanisms controlling isotopic bond ordering in abiotic and
697   biotic methane gases. *Geochim Cosmochim Acta* 2017;**203**:235–64.

698   Zehnder AJ, Brock TD. Methane formation and methane oxidation by methanogenic
699   bacteria. *J Bacteriol* 1979;**137**:420–32.

700